References

BOL'SHUTKIN, N. D., GASAN, V. M., PROKHVALTILOV, A. I. & ERENBURG, A. I. (1972). *Acta Cryst.* B**28**, 3542–3547.
KIHARA, T. (1963). *Acta Cryst.* **16**, 1119–1123.
KIHARA, T. (1966). *Acta Cryst.* **21**, 877–879.
KIHARA, T. (1970). *Acta Cryst.* A**26**, 315–320.
KIHARA, T. (1975). *Acta Cryst.* A**31**, 718–721.
KIHARA, T. & SAKAI, K. (1978). *Acta Cryst.* A**34**, 326–329.
KOSKI, H. K. & SÁNDOR, E. (1975). *Acta Cryst.* B**31**, 350–353.
SWENSON, C. A. (1955). *J. Chem. Phys.* **23**, 1963–1964.

Acta Cryst. (1981). A**37**, 51–61

Irradiation-Induced Defects in β''-Alumina Examined by 1 MV High-Resolution Electron Microscopy

BY YOSHIO MATSUI AND SHIGEO HORIUCHI

National Institute for Researches in Inorganic Materials, Sakura-mura, Niihari-gun, Ibaraki 305, *Japan*

(*Received* 26 *April* 1979; *accepted* 26 *June* 1980)

Abstract

The defect blocks formed in β''-alumina by electron irradiation are examined by 1 MV high-resolution electron microscopy. In order to explain the fact that two distinctly different types of defect images appear even in a single 1 MV micrograph, a new structural model is constructed in place of the two models so far reported. In the model proposed, two spinel-like blocks on either side of the eliminated conduction plane are directly combined by the vectors including x,y components to form cubic close packing of oxygen layers in the resultant defect blocks. The arrangements of cations in the defect block are slightly different from those expected from the spinel structure.

Introduction

The name β''-alumina was first used by Yamaguchi & Suzuki (1968) for the compound $Na_2O.5Al_2O_3$ (or $K_2O.5Al_2O_3$), because the crystal structure was substantially similar to that of β-alumina, $Na_2O.11Al_2O_3$. It was later found that the β''-alumina phase is considerably stabilized by the addition of a small amount of MgO and even single crystals have been prepared (Bettman & Peters, 1969; Kummer, 1972). Such MgO-stabilized β''-alumina, $Na_2O.MgO.5Al_2O_3$, has the idealized crystal structure as shown in Fig. 1(*a*) and (*b*) (Bettman & Peters, 1969). It is constructed by the alternate stacking of the spinel-like blocks and so-called conduction planes which consist of Na_2O. The space group is $R\bar{3}m$ (a = 5·614 and c = 33·85 Å), and the unit cell contains three spinel-like blocks which are mutually related by

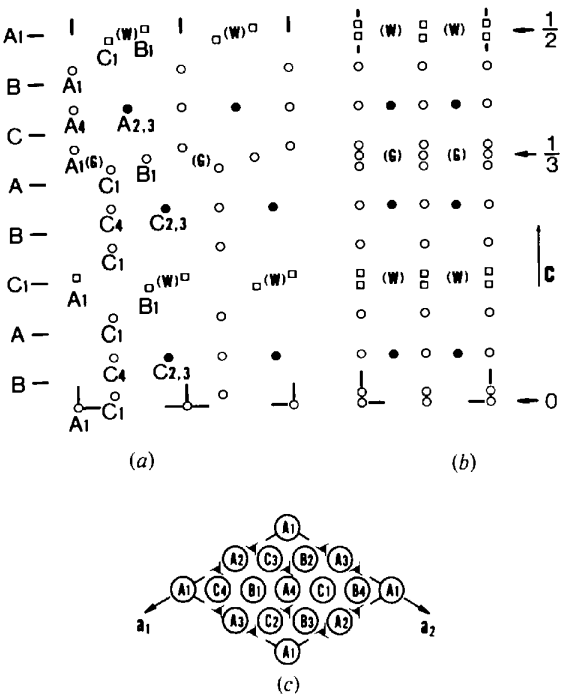

Fig. 1. Schematic representations of the crystal structure of MgO-stabilized β''-alumina, $Na_2O.MgO.5Al_2O_3$. The space group is $R\bar{3}m$ with lattice parameters a = 5·61 and c = 33·9 Å. (*a*) and (*b*) are the projections normal to the (110) and (100) planes, respectively. Half the unit cell is shown in each figure and the remaining half can be derived from the operation of the threefold screw axes shown in (*c*). Squares mean sodium atoms. Empty and filled circles represent Al atoms partly replaced by Mg ones; cations in the full circles are arrayed twice as densely as those in the empty circles along the direction of projection. The oxygen positions are abbreviated but their stacking sequence is indicated at the left-hand side of (*a*). The (x,y) coordinates of each atom can be read out from (*c*).

0567-7394/81/010051-11$01.00

the threefold screw axes parallel to the [001] direction. Each spinel-like block is composed of four cubic-close-packed oxygen layers. Oxygen atoms in the conduction planes are packed only one-quarter as densely as those in the spinel-like blocks. Using the symbols for x,y positions in Fig. 1(c), the oxygen layer sequence along the c axis is described as

$$\ldots A_1\,(CBAC)\,B_1\,(ACBA)\,C_1\,(BACB)\,A_1\ldots,$$

where the letters in parentheses stand for the oxygens in the spinel-like blocks. The sign A, for example, means that the positions A_1 to A_4 in Fig. 1(c) are all occupied. The mean distance between two neighbouring oxygen layers is about 2·3 Å. The thickness of each block, *i.e.* the separation between adjoining conduction planes, is about 11·3 Å. Two spinel-like blocks are linked by Al–O–Al bridges, where O is the oxygen in the conduction plane. The Al atom in the bridge is surrounded tetrahedrally by four oxygens, one in the conduction plane and three in the spinel-like block.

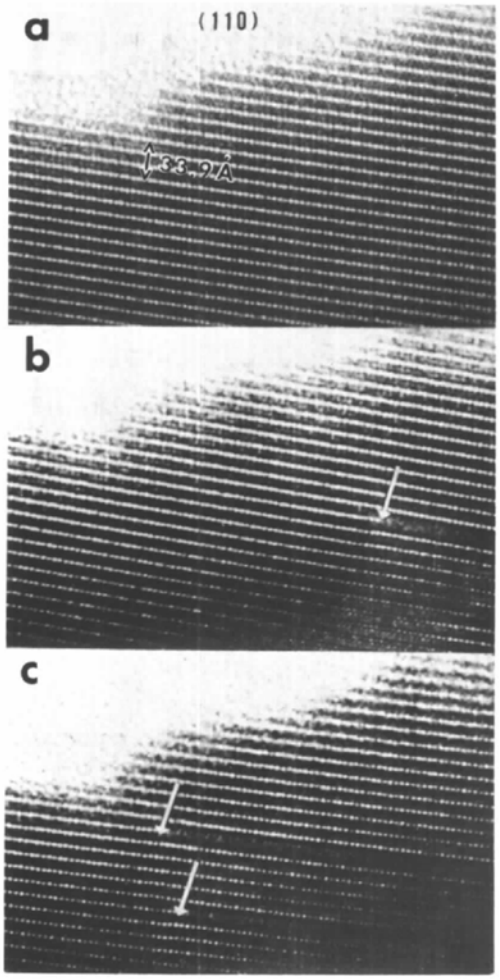

Fig. 2. 100 kV electron micrographs showing the time sequence of the development of the irradiation-induced defects in β''-alumina.

Recently, high-resolution electron microscopy has successfully been applied in characterizing the imperfections in β- as well as β''-alumina (Bevan, Hudson & Moseley, 1974; Sato & Hirotsu, 1976; De Jonghe, 1979). In the case of β''-alumina, however, the crystal is known to be very sensitive to electron irradiation; some conduction planes are easily eliminated leaving the defect blocks behind (De Jonghe, 1977; Matsui & Horiuchi, 1977; Bovin, 1978, 1979), as shown in Fig. 2(a) to (c) by a series of 100 kV electron micrographs. The majority of the defect blocks thus created have the width of 20·3 Å which is 2·3 Å smaller than twice the thickness of the original spinel-like blocks (De Jonghe, 1977). This indicates that the defect blocks are formed by the direct contact of two spinel-like blocks on either side of the eliminated conduction plane. Two different models have so far been proposed on the formation mechanism and the resultant structure of the defect block. De Jonghe (1977) insisted that the structure in the defect block is the spinel type because, in his electron micrograph, two conduction planes sandwiching the defect block seemed to have the 'same' x,y positions. The oxygen layer sequence expected from this model is

$$\ldots B_1[(ACBA)(CBAC)]\,B_1\ldots.$$

Bovin (1979), on the other hand, has proposed another model in which the hexagonal close packing of oxygen layers is included. This was deduced from the observations in his electron micrograph that two conduction planes sandwiching the defect block seemed to have 'different' x,y positions. The oxygen layer sequence in this model is

$$\ldots B_1[(ACBA)(BACB)]\,A_1\ldots.$$

Matsui & Horiuchi (1977) have already reported, based on the high-resolution 1 MV electron microscope study of β''-alumina, that the defect blocks of 20·3 Å thickness sometimes show two different types of images even in a single micrograph. As explained later, one of these images corresponds to De Jonghe's and, therefore, cannot be understood by Bovin's model. The other defect image, on the other hand, corresponds to Bovin's and, therefore, cannot be understood by De Jonghe's structure model.

Because of these differences between the models so far proposed and the observed images, 1 MV high-resolution images of defect blocks reported previously (Matsui & Horiuchi, 1977) are analysed in detail in this study. We will propose a new model for the structure in the irradiation-induced defect blocks in β''-alumina. The appearance of two different types of defect images is expected naturally from our new model.

Experimental

1. *Electron microscope observations*

The sample crystal of β''-alumina was prepared by heating powders mixed with the composition 9 wt% Na_2O, 4 wt% MgO and 87 wt% Al_2O_3 at 1170 K for 1 h in air. Na_2O was added in the form of Na_2CO_3. Powder X-ray diffraction patterns showed that the product was composed only of β''-alumina. A sintered block was lightly crushed in CCl_4 and the obtained crystal fragments were set on a holey carbon film. Observations were made by a Hitachi H-1250 high-resolution electron microscope with a goniometer ($\pm 35°$ tilt) operated at 1 MV. Details on this instrument are presented elsewhere (Horiuchi, Matsui, Bando, Katsuta & Matsui, 1978). Through-focus series of images were taken with the incident beam normal to the (110) as well as the (100) planes of β''-alumina. The objective aperture employed in imaging corresponds to 0·56 $Å^{-1}$ in reciprocal space. It has already been shown that 1 MV images taken at about 1000 Å underfocus approximately reflect the projected potential of crystals (Horiuchi & Matsui, 1974; Horiuchi, Muramatsu & Matsui, 1978). The above imaging conditions are in accord with the principles of electron optics (Scherzer, 1949; Cowley & Iijima, 1972; Fejes, 1977). In order to prevent abrupt changes of β''-alumina structure upon electron irradiation, the intensity of the electron beam was maintained at the minimum level necessary for observing at the direct magnification of about 2×10^5 times.

2. *Computer simulations of image contrast*

Amplitudes of the scattered electron waves were first calculated for β''-alumina structure (Bettman & Peters, 1969). Effects of the crystal thickness were dynamically treated by the multi-slice method (Cowley & Moodie, 1957; Goodman & Moodie, 1974). The number of waves taken into account in the calculations were 465 and 297 for projections normal to the (110) and the (100) planes, respectively. The thickness of the unit slice was 5·61 and 4·85 Å respectively.

Image contrasts were then calculated taking into account the effects of the spherical aberration of the objective lens, amount of defocus and the size of the objective aperture. According to the size of the aperture mentioned before, 53 and 31 waves contribute for imaging in each case. Chromatic aberration was taken into account after Fejes (1977); the effect is treated as due to the fluctuations of the defocus approximated by a Gaussian distribution with a standard deviation Δ about a mean defocus. It has already been clarified that suitable values for Δ and C_s, the spherical aberration coefficient, are about 400 Å and 10 mm, respectively, for the present 1 MV electron microscope (Horiuchi, Muramatsu & Matsui, 1978).

Experimental results and interpretation

1. 1 MV *images of* β''*-alumina and irradiation-induced defects*

The examples of the through-focus series of 1 MV electron micrographs of β''-alumina projected onto the (110) plane are shown in Fig. 3(*a*) to (*c*). They are taken at about 500, 1000 and 1500 Å underfocus, respectively. The image in each micrograph is composed of rows of white dots lying normal to the *c* axes and the contrasts are not greatly affected by the variations in defocus, at least in the above ranges. This substantially agrees with the results of the computer simulations shown in Fig. 4(*a*) to (*e*) for various defocus values (for common thickness of about 34 Å). It is also noticed from Fig. 3(*a*) to (*c*) that the variation of image contrast with crystal thickness is not so large and this again agrees with the calculations for thicker cases as shown in Fig. 8(*a*) and (*c*). The high-magnification micrograph corresponding to 1000 Å underfocus is shown in Fig. 5. According to the calculations so far mentioned, each large white dot in Fig. 5 is interpreted as corresponding to the midpoints of two adjoining sodium positions in the conduction planes, *W* in Fig. 1(*a*). If there is no chromatic aberration, *i.e.* if $\Delta = 0$, the calculated image, for 34 Å thickness and 1000 Å underfocus, is as shown in Fig.

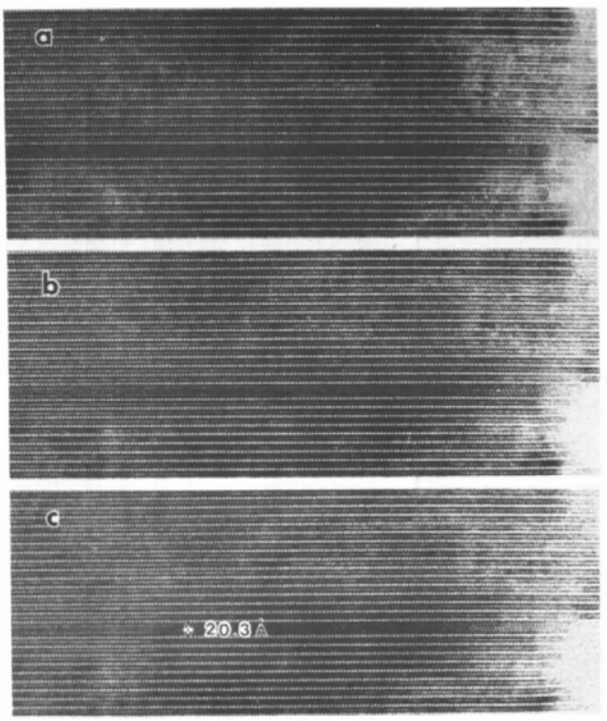

Fig. 3. The through-focus series of 1 MV electron micrographs of β''-alumina taken at an underfocus of about (*a*) 500 Å, (*b*) 1000 Å and (*c*) 1500 Å. The electron beam is incident on the (110) plane.

4(f). It may be understood from this calculation that the appearances of large white dots in Fig. 5 are mainly the results of the lowering of the resolution due to the chromatic aberration. In each line of white dots, two adjoining dots are mutually separated by 4·85 Å (a cos 30°). Two neighbouring lines, separated by 11·3 Å, are mutually displaced, normal to the c axes, by $\frac{1}{3}$ of 4·85 Å, in agreement with the presence of the threefold screw axes in the β''-alumina structure. The grey, or weak white, dots in Fig. 5 are considered to correspond to the midpoints of two tetrahedral cations in the central part of the spinel-like blocks, G in Fig. 1(a).

In both Fig. 3 and Fig. 5, the irradiation-induced defects of 20·3 Å width are observed. As already pointed out (Matsui & Horiuchi, 1977), the most important fact is that there are two distinctly different types of defect images, P and Q, in Fig. 5. According to our measurements, the upper white dots are just above the lower ones at P. At Q, on the other hand, the upper white dots are just above the midpoints of two adjacent lower ones. In other words, the upper and the lower lines of white dots are mutually displaced, normal to the c axis, by $\frac{1}{2}$ of 4·85 Å at Q, while there are no such displacements at P. The defect image previously reported by De Jonghe (1977), which is shown in Fig. 5 of his paper, may correspond to our P-type one. That reported by Bovin (1979), shown in Fig. 5 of his paper, may correspond to our Q-type one.

A 1 MV image of β''-alumina, taken with the beam normal to the (100) plane, is shown in Fig. 6. The image was taken at about 1000 Å underfocus. As shown in Fig. 7(b) to (d), the calculated images for 750, 1000 and 1250 Å underfocus are in good agreement with the real image in Fig. 6. This holds also for the thicker cases as shown in Fig. 8(b) and (d). According to these calculations, the white and grey dots in Fig. 6 are interpreted as corresponding to the sites W and G in Fig. 1(b), respectively.

Two types of defect images, P' and Q', are also observed in Fig. 6. The accurate measurements of the positions of white dots around the defect blocks are difficult because the image is less sharp than the image in Fig. 5. It is, however, appreciated that the upper and lower lines of white dots are arranged almost in the

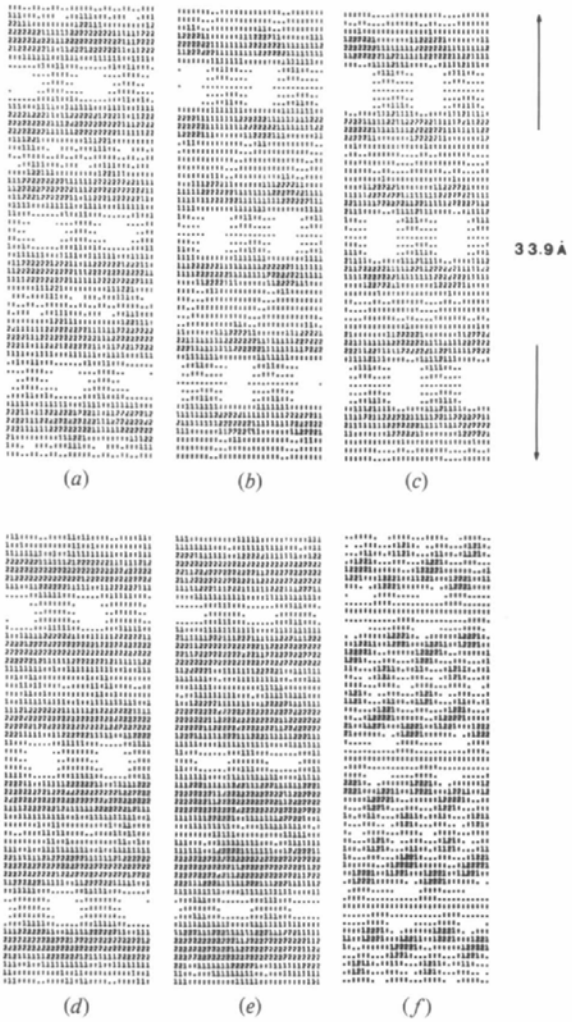

Fig. 4. The calculated images of β''-alumina projected onto the (110) plane. The values of defocus are assumed to be (a) 500 Å, (b) 750 Å, (c) 1000 Å, (d) 1250 Å and (e) 1500 Å. The crystal thickness is about 34 Å (six times unit-slice thickness). Δ is 400 Å. For (f), Δ is assumed to be 0 Å with an underfocus of 1000 Å.

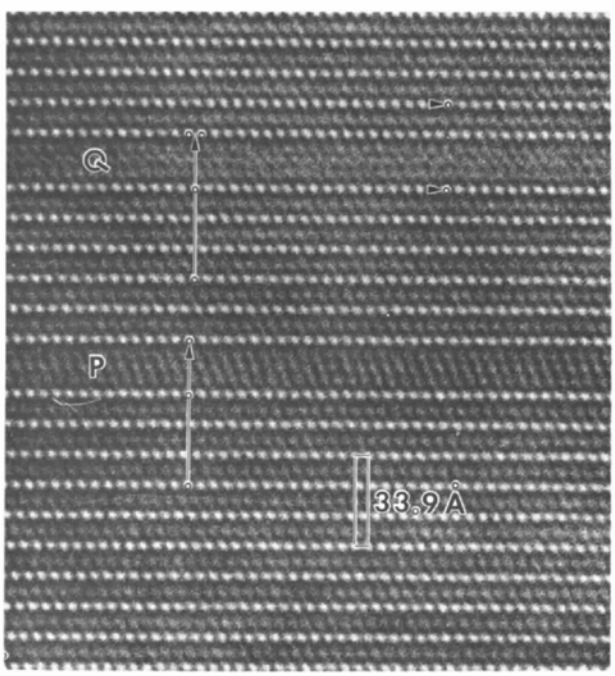

Fig. 5. High-magnification 1 MV image of β''-alumina projected onto the (110) plane. Two kinds of irradiation-induced defects, P and Q, are clearly observed. Arrows are drawn to show that the relative positions of white dots on either side of the defect blocks are different for P and Q.

same way at P', while they are arranged obliquely at Q'. In the following analyses, the structure in the defect block is examined based mainly on the sharp images in Fig. 5. Those in Fig. 6 are then used for checking the structural model obtained.

2. *Determinations of the slide vectors*

In this section, we analyse how the upper and lower spinel-like blocks are mutually shifted and then combined to form the defect block after the loss of the conduction plane between them. The vectors, tentatively named as 'slide vectors', by which the relative movements of the upper block with respect to the lower one are described, are determined as follows.

As stated before, the oxygen layer sequence in β''-alumina is

(lower region)$\ldots B_1(ACBA)C_1(BACB)A_1\ldots$(upper region).

It may be expected that the oxygens are also close packed in the defect block formed after the loss of the conduction plane C_1. There are then two possibilities for the oxygen sequence in the defect block. The first one is the sequence $[(ACBA)(BACB)]$, which arises from the simple contact between two spinel-like blocks. This model corresponds to that of Bovin (1979). The second possibility is the sequence $[(ACBA)(CBAC)]$, for which two spinel-like blocks must mutually be shifted in the (001) plane during the collapse. The first stacking is composed of cubic and hexagonal close packing, but the latter only of cubic close packing.

According to the first, *i.e.* Bovin's, model, two crystal regions on either side of the lost conduction plane, C_1, are combined directly along the c axis. The slide vector is then expressed approximately as

$$\mathbf{V}_c \simeq -\tfrac{1}{15}\,\mathbf{c}$$

where $\mathbf{c}$ is the lattice vector of β''-alumina. The absolute value of $\mathbf{V}_c$ is about 2·3 Å, corresponding to the distance between two neighbouring oxygen layers. The oxygen sequence in the defect block thus created is

$$\ldots B_1[(ACBA)(BACB)]\,A_1\ldots.$$

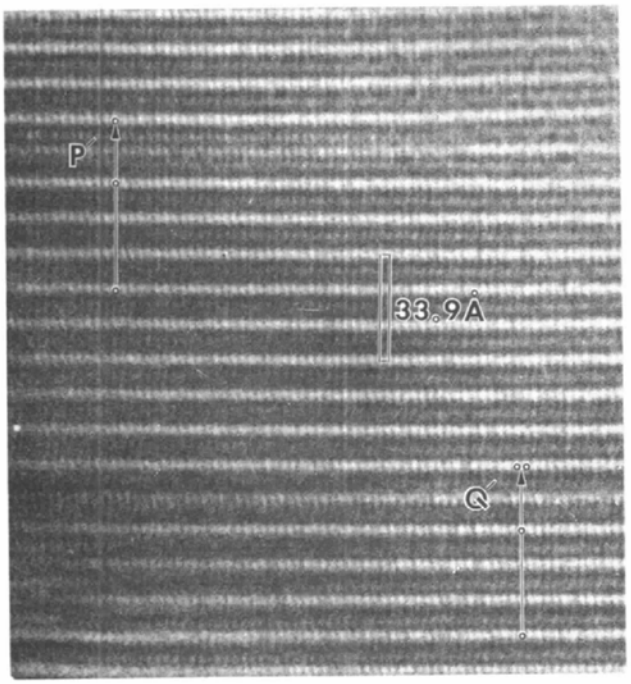

Fig. 6. High-magnification 1 MV electron micrograph of β''-alumina projected onto the (100) plane. Two kinds of images of irradiation-induced defects, P' and Q', are observed.

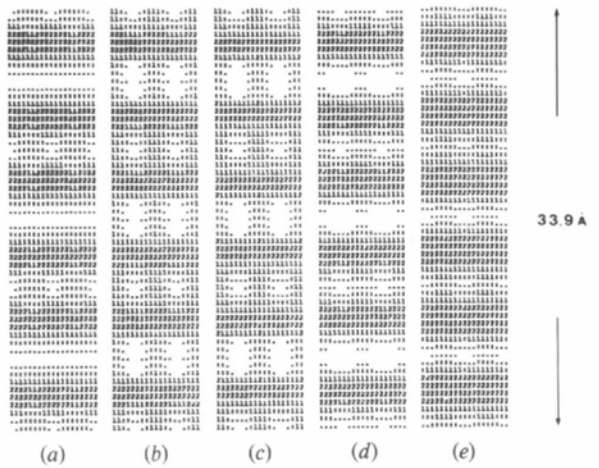

Fig. 7. The calculated images of β''-alumina projected onto the (100) plane. The values of defocus are assumed to be (*a*) 500 Å, (*b*) 750 Å, (*c*) 1000 Å, (*d*) 1250 Å and (*e*) 1500 Å. The crystal thickness is assumed to be about 34 Å (seven times unit-slice thickness). Δ is 400 Å.

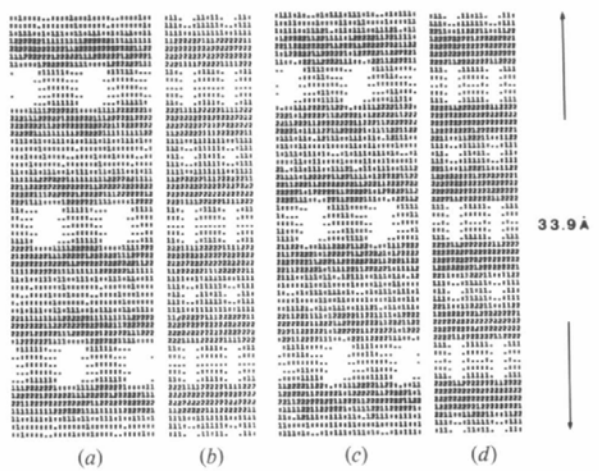

Fig. 8. The calculated images of β''-alumina. The crystal thickness is assumed to be about 67 Å in (*a*) and (*b*) and about 100 Å in (*c*) and (*d*). (*a*) and (*c*) are the projections normal to the (110) plane and (*b*) and (*d*) the projections normal to the (100) plane.

This means that both lines of white dots corresponding to the upper and lower conduction planes, A_1 and B_1, must mutually be displaced, normal to the c axis, by $\frac{1}{3}$ of 4·85 Å, when they are projected onto the (110) plane. As already shown in Fig. 5, however, there are no such displacements for P but there are $\frac{1}{2}$ displacements for Q, respectively. The simple contact model of Bovin (1979) is, therefore, inadequate to explain the real observations of the defect blocks.

According to the second model, we can explain the image in Fig. 5 if we assume the cases where the cubic close packing of oxygens is attained through the minimum slide vectors. There are three such vectors, $\mathbf{V}_i$ (i = 1 to 3), which are schematically shown in Fig. 9. They are also expressed as

$$\mathbf{V}_1 \simeq \tfrac{1}{6}\mathbf{a}_1 + \tfrac{1}{3}\mathbf{a}_2 + \mathbf{V}_c$$
$$\mathbf{V}_2 \simeq -\tfrac{1}{3}\mathbf{a}_1 - \tfrac{1}{6}\mathbf{a}_2 + \mathbf{V}_c$$
$$\mathbf{V}_3 \simeq \tfrac{1}{6}\mathbf{a}_1 - \tfrac{1}{6}\mathbf{a}_2 + \mathbf{V}_c$$

where $\mathbf{a}_1$ and $\mathbf{a}_2$ are also the lattice vectors of β''-alumina. $\mathbf{V}_1$, $\mathbf{V}_2$ and $\mathbf{V}_3$ are mutually related by 120° rotations around the c axis and, therefore, they are crystallographically equivalent because the crystal of β''-alumina had originally threefold rotational symmetry. The defect blocks created by the above three slide vectors must, then, be structurally the same except for their orientations with respect to the host β''-alumina lattice. The oxygen layer sequence in the defect block thus created is

$$\ldots B_1[(ACBA)(CBAC)]\,B_j \ldots$$

where j is 2, 3 or 4 depending on which one of three vectors $\mathbf{V}_i$(i = 1, 2 or 3) were actually employed in creating each defect block. If the defect block was formed through $\mathbf{V}_3$ (j = 4 in above sequence), both conduction planes, B_1 and B_4, may be imaged as if they have the same x,y positions when they are projected normal to the (110) plane. In other words, the image of type P in Fig. 5 is expected from the defect block formed through $\mathbf{V}_3$. The image taken by De Jonghe (1977) might correspond to this case. If, on the other hand, the defect block was created through the slide vector $\mathbf{V}_1$ or $\mathbf{V}_2$ (j = 2 or 3 in above sequence), both conduction planes, B_1 and B_2 (or B_1 and B_3), must be imaged as if they are mutually displaced by $\frac{1}{2}$ of 4·85 Å

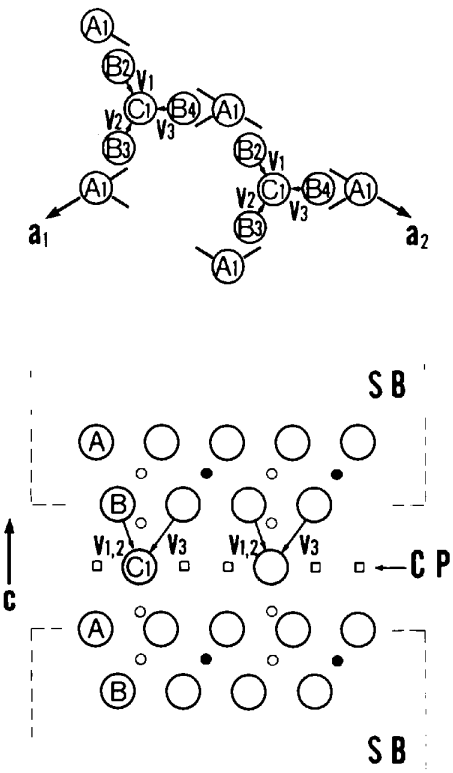

Fig. 9. Schematic representations of the slide vectors $\mathbf{V}_i$ (i = 1 to 3) which describe the movements of the upper spinel-like block (SB) with respect to the lower one. Squares are sodium atoms in the conduction plane (CP), which is subsequently eliminated upon electron irradiation. Empty and solid small circles have the same meaning as in Fig. 1. Large empty circles represent the oxygen atoms. Upper and lower figures show the projections parallel and normal to the [001] direction, respectively.

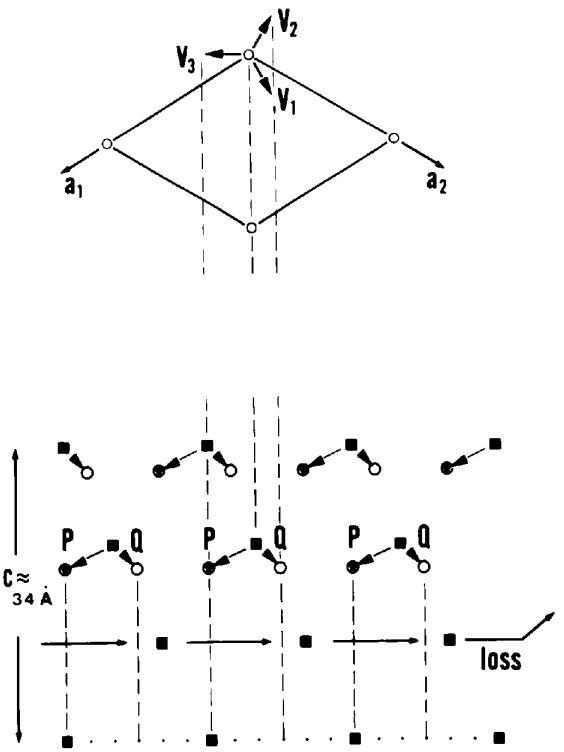

Fig. 10. Schematic representations of the positional changes of the white dots when irradiation-induced defects are created in β''-alumina. Solid squares stand for the original white dots in the image of β''-alumina projected onto the (110) plane. The signs ▼ and ○ correspond to the P and Q types of defect image, respectively. The vertical scale is artificially reduced to make the figures more easily perceived.

when they are projected normal to the (110) plane. In other words, the image of type Q in Fig. 5 is expected from $\mathbf{V}_1$ or $\mathbf{V}_2$. The images taken by Bovin (1979) might correspond to this case, although he interpreted the image based on the mutual displacements of white dots by $\frac{1}{3}$ of 4·85 Å. Comments on this point will be given later. The schematic representations of the changes of the positions of white dots in the case of each of the three slide vectors are drawn in Fig. 10. The arrangements of white dots expected from De Jonghe's (1977), Bovin's (1979) and the present models are also presented in Fig. 11 (*a*), (*b*) and (*c*), respectively.

The appearance of two types of defect images, P' and Q', in Fig. 6 can also be explained by our model. It is obvious from Fig. 1(*c*) that the positions B_1 and B_3 cannot be distinguished for the projection normal to the (100) plane. Therefore the image of type P' is expected from the defect block formed through $\mathbf{V}_2$. Similarly, the image of type Q' is expected from the defect block formed through $\mathbf{V}_1$ ($j = 2$) or $\mathbf{V}_3$ ($j = 4$) because the positions B_1 and B_2 (or B_1 and B_4) may be imaged as if they are mutually displaced by $\frac{1}{2}$ of 2.8 Å when projected onto the (100) plane.

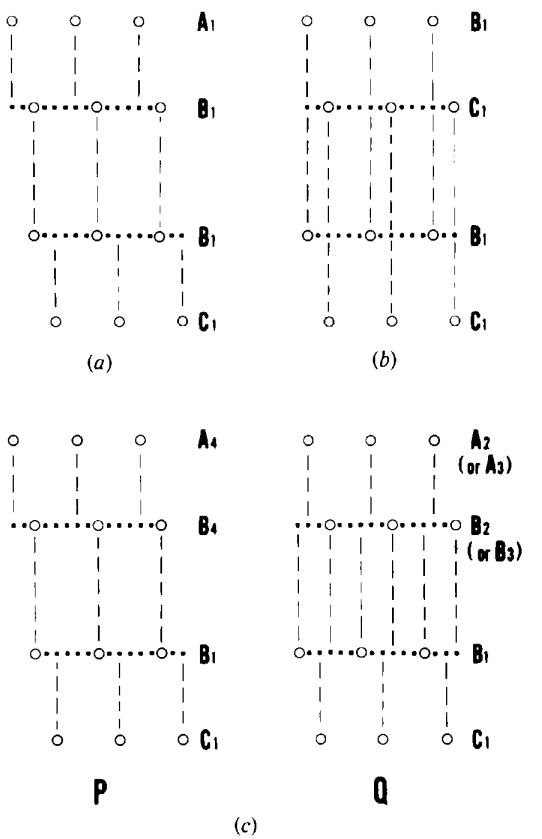

Fig. 11. Schematic representations of the arrays of white dots on either side of the irradiation-induced defect blocks expected from (*a*) De Jonghe's, (*b*) Bovin's and (*c*) the present model. The vertical scale is artificially reduced.

The types of images expected for each of the slide vectors are summarized in Tables 1 and 2 which show the cases of the projections normal to the {110} and the {100} planes, respectively.

3. *Possible structure model of irradiation-induced defects*

The structure in the defect block derived from the slide vectors mentioned above is shown in Fig. 12, where diagrams (*a*) and (*b*) correspond to the images P and Q in Fig. 5 and diagrams (*c*) and (*d*) to the images P' and Q' in Fig. 6, respectively. The meaning of the arrows drawn in the central part of each diagram will be explained in due course.

Firstly, we calculated the image contrasts of the defect blocks based on the structure derived only from the slide vectors $\mathbf{V}_1$, $\mathbf{V}_2$ or $\mathbf{V}_3$. As shown in Fig. 13(*a*) and (*b*) for the examples of P and Q', however, the matching with the real images in Fig. 5 (for P) and Fig. 6 (for Q') is not so good. For example, the continuous white line in the central part of the calculated Q' in Fig. 13(*b*) does not agree with the real observations in Fig. 6 where the white dots are observed in the central part of Q'. We consider that the gaps between the calculated and the real images indicate that some further atomic rearrangements may occur especially in the central part of the irradiation-induced defect blocks. Possibilities of such rearrangements are also suggested from following crystal-chemical considerations.

As mentioned earlier, two spinel-like blocks in β''-alumina were originally linked by Al–O–Al bridges, forming the corner sharing of two AlO_4 tetrahedra. When the mutual shifts described by the slide vectors so far mentioned are applied to these two tetrahedra,

Table 1. *The classification of the types of electron-microscope images of irradiation-induced defects, in terms of the slide vectors* $\mathbf{V}_i$ ($i = 1$ to 3) *and the projection planes* (110), (1$\bar{2}$0) *and* (2$\bar{1}$0)

P and Q correspond to those shown in Fig. 5.

	(110)	(1$\bar{2}$0)	(2$\bar{1}$0)
$\mathbf{V}_1$	Q	Q	P
$\mathbf{V}_2$	Q	P	Q
$\mathbf{V}_3$	P	Q	Q

Table 2. *Classification of the types of electron-microscope images for the cases where the defect blocks are projected onto the* (100), (010) *and* (1$\bar{1}$0) *planes of the host lattice*

P' and Q' correspond to those shown in Fig. 6.

	(100)	(010)	(1$\bar{1}$0)
$\mathbf{V}_1$	Q'	P'	Q'
$\mathbf{V}_2$	P'	Q'	Q'
$\mathbf{V}_3$	Q'	Q'	P'

the result is the edge sharing of two tetrahedra. Such a polyhedral relation is, however, known to be unstable (Pauling, 1960), due to the electrostatic repulsion force between two cations. Some rearrangements of these two Al atoms are, therefore, reasonably expected. Although there are many theoretically possible ways for such rearrangements, we consider that the most probable are the movements from the tetrahedral positions to the neighbouring octahedral vacant ones as schematically shown in Fig. 14. These Al movements are also shown by arrows in Fig. 12(*a*) to (*d*). Here, we

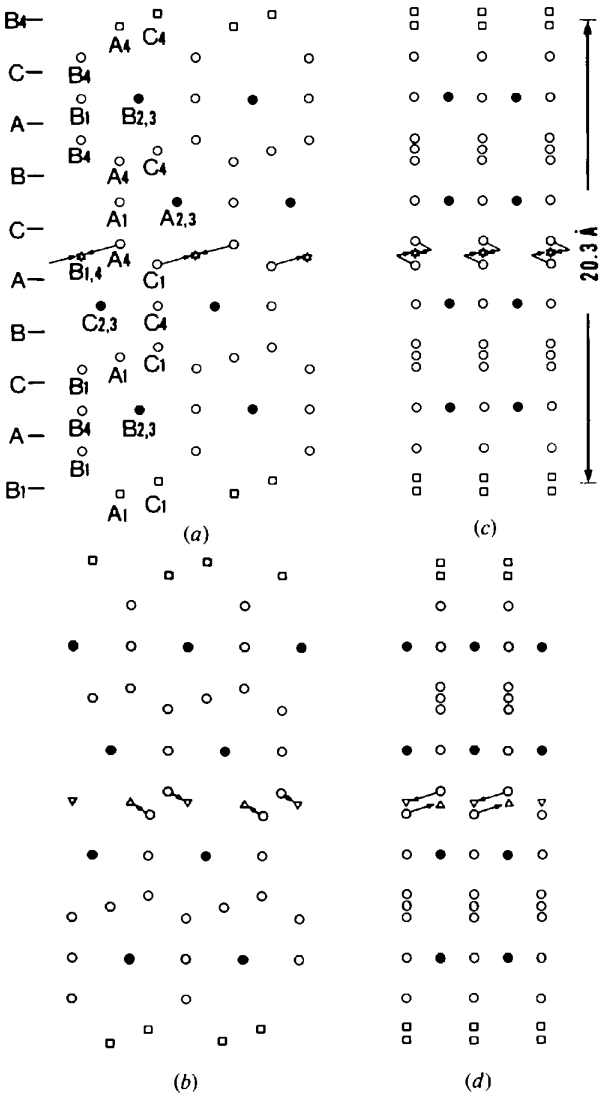

Fig. 12. The structure model of an irradiation-induced defect block of 20·3 Å width formed in β''-alumina. In this figure, the defect block formed through the slide vector $\mathbf{V}_3$ is assumed. (*a*) to (*d*) are, therefore, the projections onto the (110), (1$\bar{2}$0) [or (2$\bar{1}$0)], (1$\bar{1}$0) and (100) [or (010)] planes of the host β''-alumina lattice. They correspond to the image types *P*, *Q*, *P'* and *Q'* in Figs. 5 and 6, respectively. Triangles represent the Al positions after the rearrrangements in the central part of the defect block which is shown in Fig. 14.

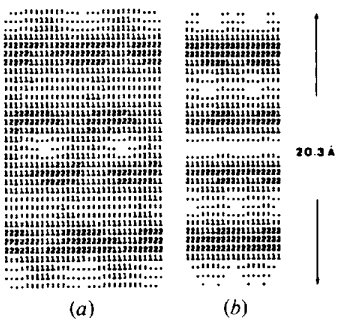

Fig. 13. The results of the calculations of the defect images *P* and *Q'*. Crystal thickness is assumed to be about 34 Å. The Al movements shown in Figs. 12 and 14 are not taken into account.

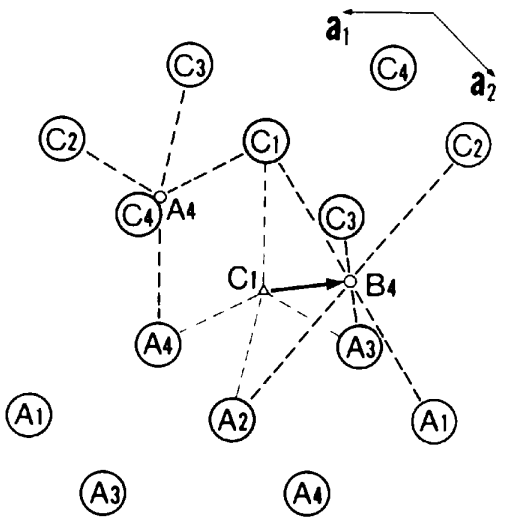

Fig. 14. Schematic representations of the movement of an Al atom from the tetrahedral position (C_1) to the octahedral one (B_4). The defect block initially formed through $\mathbf{V}_3$ is assumed in the figure.

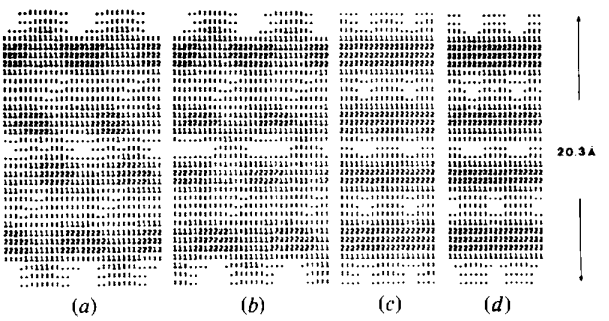

Fig. 15. The calculated images of the defect block corresponding to *P*, *Q*, *P'* and *Q'* in (*a*) to (*d*), respectively. The rearrangements of Al atoms shown in Figs. 12 and 14 are taken into account; the probabilities for $C_1 \rightarrow B_4$ and $A_4 \rightarrow B_1$ movements are assumed to be 30 and 50%, respectively. The crystal thickness is 34 Å.

consider the defect block formed through $\mathbf{V}_3$. If one of the pair of two tetrahedral Al atoms, for example that at C_1, moved to the neighbouring B_4 position, corner sharing between an AlO_4 tetrahedron and an AlO_6 octahedron is created. If another Al atom, at an A_4 site, also moved to the octahedral B_1 position, the edge sharing between two octahedra is created. Anyway, the resultant polyhedral relations in the central part of the defect block may be more stable than the edge sharing of two tetrahedra derived directly through the slide vectors.

Then we tried to calculate the 1 MV images of the defect blocks by varying the probabilities of $A_4 \rightarrow B_1$ and $C_1 \rightarrow B_4$ movements of Al atoms in the central part of the defect block. Positions of other atoms in the defect block are just those derived directly from the slide vector. Substantial agreements with the real images in Figs. 5 and 6 are obtained when we assume that the probabilities of Al movements mentioned above are 30–50%. The examples of the calculated images for P, Q, P' and Q' types of defect images are shown in Fig. 15(*a*) to (*d*), respectively.

Discussions

1. *Comparisons with previously proposed models*

(*a*) *De Jonghe's spinel model.* The spinel model of De Jonghe (1977) is, as mentioned before, considered to be derived from the image corresponding to our P-type one. The existence of the Q type of image in Fig. 5 cannot be explained by this model at all. The problem remains, however, of how we can prove that P cannot be attributed to the spinel lamella. In order to solve this problem, we performed the following observations. Figs. 16(*a*) and 16(*b*) are the projections onto the (110) and the (100) planes, respectively, taken from exactly the same crystal region. The defect blocks 1 and 2 are both imaged as P type in Fig. 16(*a*). They are, however, imaged as Q' type in Fig. 16(*b*). This cannot be explained by the spinel model because the upper and lower conduction planes must have exactly the same x,y positions in this model and, therefore, only the P' type of image is expected in Fig. 16(*b*).

According to our new model, the defect blocks 1 and 2 are both formed through the slide vector $\mathbf{V}_3$. As summarized in Tables 1 and 2, they are expected to be imaged as P type when projected onto the (110) plane and as Q' type when projected onto the (100) [or (010)] plane after tilting by 30° around the c axis.

It may be noted that the slide vector proposed by De Jonghe (1977), shown by an arrow in the insert in Fig. 5 of his paper, is essentially the same as one of our three slide vectors. Unfortunately, however, he was mistaken in proposing that the structure derived from such a vector is the spinel type.

(*b*) *Bovin's structure model.* Bovin's (1979) proposal on the irradiation-induced defects in β''-alumina is, as pointed out before, considered to be derived from the image corresponding to our Q-type one and the existence of the P-type image in Fig. 5 cannot be explained by his model at all. Moreover, Bovin's interpretation of the Q-type image is different from ours; according to him, both lines of white dots sandwiching the defect block are mutually displaced, normal to the c axis, by $\frac{1}{3}$ of 4·85 Å (as shown in Fig. 11*b*), while we consider that they are displaced by $\frac{1}{2}$ of 4·85 Å (as shown in Fig. 11*c*). It may, therefore, be useful to point out some facts which cannot be explained by Bovin's image interpretations.

The oxygen layer sequence expected from Bovin's model is

$$\ldots A_1(CBAC)\,B_1[(ACBA)(BACB)]\,A_1(CBAC)\,B_1\ldots,$$

indicating that white dots marked by arrows in the upper right part of Fig. 5 must be at the same x,y positions. They are, however, slightly displaced relative to each other. It can be seen that the amount of the displacement is smaller than $\frac{1}{3}$ of 4·85 Å, on comparing with the mutual arrangements of white dots in a host

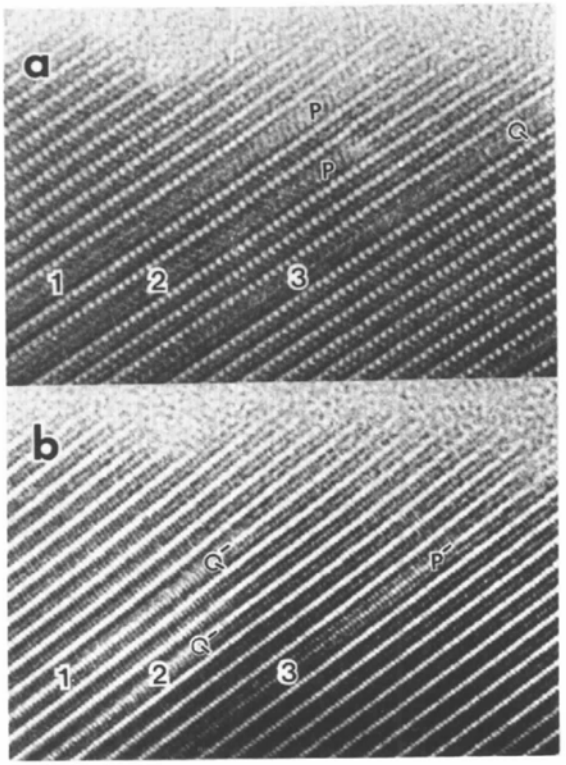

Fig. 16. 1 MV electron micrographs of irradiation-induced defects in β''-alumina projected onto the (110) and the (100) planes in (*a*) and (*b*), respectively. Experimentally, (*b*) was taken first and then (*a*) was taken after the crystal was tilted by 30° around the c axis. According to our model, the defect blocks 1 and 2 are both created through $\mathbf{V}_3$, while 3 is created through $\mathbf{V}_2$.

β''-alumina lattice where the $\frac{1}{3}$ displacements are secured by the presence of the threefold screw axes. According to our new model, on the other hand, the oxygen layer sequence near the Q-type image is

$$\ldots A_1(CBAC)\,B_1[(ACBA)(CBAC)]\,B_2(ACBA)\,C_2\ldots,$$

if the defect block was formed through $\mathbf{V}_1$. The positions A_1 and B_2 (or B_1 and C_2) are expected to be mutually displaced by $\frac{1}{6}$ of 4·85 Å when projected normal to the (110) plane.

The second example, which cannot be explained by Bovin's model, is shown in Fig. 17, where two Q-type defect images are observed accidentally side by side.

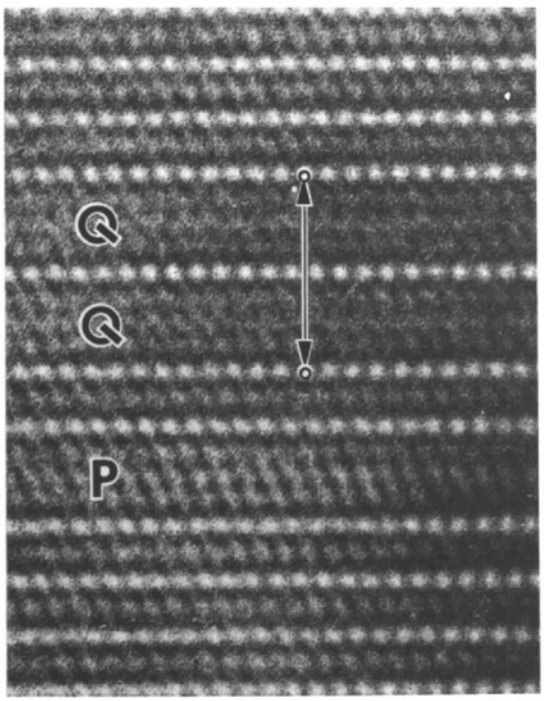

Fig. 17. The 1 MV electron micrograph of the (110) projection, showing the special case where two Q-type defect images are observed accidentally side by side.

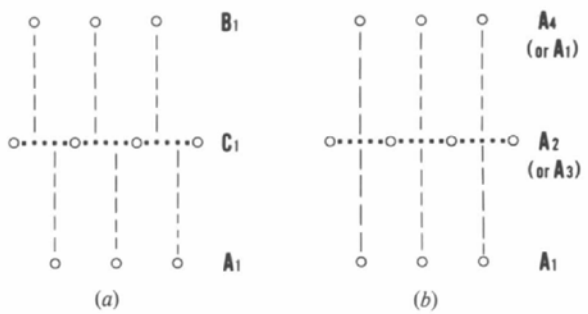

Fig. 18. Schematic representations of the arrays of white dots in Fig. 17 expected from (*a*) Bovin's and (*b*) the present structure model.

According to Bovin's model, the oxygen layer sequence in such a region must be

$$\ldots A_1[(CBAC)(ACBA)]\,C_1[(BACB)(CBAC)]\,B_1\ldots,$$

indicating that the first and the third conduction planes (A_1 and B_1), marked by an arrow in Fig. 17, must be displaced, normal to the c axis, by $\frac{1}{3}$ of 4·85 Å, as schematically shown in Fig. 18(*a*). These two planes are, however, arranged almost in the same way; no mutual displacements are observed for two lines of white dots linked by an arrow in Fig. 17. According to our new model, the oxygen layer sequence in the corresponding area is

$$\ldots A_1[(CBAC)(BACB)]\,A_2[(CBAC)(BACB)]\,A_4\ldots,$$

if both defect blocks were formed through $\mathbf{V}_2$. If the first defect block was formed through $\mathbf{V}_2$ and the second one by $\mathbf{V}_1$, the oxygen layer sequence is

$$\ldots A_1[(CBAC)(BACB)]\,A_2[(CBAC)(BACB)]\,A_1\ldots.$$

In any case, the first and third conduction planes are expected to be imaged as if they have the same x,y positions when they are projected normal to the (110) plane. The schematic representation of the arrays of white dots by our model is shown in Fig. 18(*b*). The real observations in Fig. 17 are thus reasonably understood on the basis of our structure model.

Appearances of the Q' type of defect image in Fig. 6 also cannot be explained by Bovin's model, because the positions A_1, B_1 and C_1 cannot be distinguished when projected onto the (100) plane and, therefore, only the P' type of image is always expected in Fig. 6 from Bovin's structure model.

2. *Electron damage in other related materials*

The formation of electron-induced defects has so far not been reported for β-alumina ($Na_2O.11Al_2O_3$) and β'''-alumina ($Na_2O.4MgO.15Al_2O_3$) which has hexagonal symmetry. Such phenomena were, however, reported for β''''-alumina ($Na_2O.3MgO.7Al_2O_3$) (Matsui, Horiuchi & Ohta, 1980). This compound has almost the same crystal structure as β''-alumina except that each spinel-like block is composed not of four but of six close-packed oxygen layers (Weber & Venero, 1970). In this case, the defect block of about 30 Å width is created by electron irradiation. Two types of image are also observed which have been reasonably explained in a similar manner to that for β''-alumina in the present study. The detailed analyses on β''''-alumina will be given elsewhere (Matsui, 1981).

3. *Note on non-stoichiometry*

The effects of the point defects, associated with the non-stoichiometry in β''-alumina (Bettman & Peters, 1969), on the formation of irradiation-induced defects

remain unsolved. Such discussions may be difficult at the present stage because even the structural defects in original β''-alumina have so far not been satisfactorily clarified. It is, however, our opinion that the essential points of our results deduced from the idealized crystal structure of β''-alumina may hold substantially unchanged even for real, non-stoichiometric β''-alumina.

The authors wish to express their deep gratitude to Drs A. Imai, M. Harata and T. Ohta (Toshiba Research and Development Center) for the preparation of the sample crystals and to Drs K. Kato and Y. Bando (NIRIM) for valuable discussions. They also thank Messrs Y. Sekikawa and K. Sakaguchi (NIRIM) for their help in high-resolution HVEM experiments.

References

BETTMAN, M. & PETERS, C. R. (1969). *J. Phys. Chem.* **73**, 1774–1780.
BEVAN, D. J., HUDSON, B. & MOSELEY, P. T. (1974). *Mater. Res. Bull.* **9**, 1073–1083.
BOVIN, J. O. (1978). *Nature (London)*, **273**, 136–138.
BOVIN, J. O. (1979). *Acta Cryst.* A**35**, 572–580.
COWLEY, J. M. & IIJIMA, S. (1972). *Z. Naturforsch.* **27**, 445–451.
COWLEY, J. M. & MOODIE, A. F. (1957). *Acta Cryst.* **10**, 609–619.
DE JONGHE, L. C. (1977). *Mater. Res. Bull.* **12**, 667–674.
DE JONGHE, L. C. (1979). *J. Am. Ceram. Soc.* **62**, 289–293.
FEJES, P. L. (1977). *Acta Cryst.* A**33**, 109–113.
GOODMAN, P. & MOODIE, A. F. (1974). *Acta Cryst.* A**30**, 280–290.
HORIUCHI, S. & MATSUI, Y. (1974). *Philos. Mag.* **30**, 777–787.
HORIUCHI, S., MATSUI, Y., BANDO, Y., KATSUTA, T. & MATSUI, I. (1978). *J. Electron Microsc.* **27**, 39–48.
HORIUCHI, S., MURAMATSU, K. & MATSUI, Y. (1978). *Acta Cryst.* A**34**, 939–946.
KUMMER, J. T. (1972). *Prog. Solid State Chem.* **7**, 141–175.
MATSUI, Y. (1981). *J. Appl. Cryst.* In the press.
MATSUI, Y. & HORIUCHI, S. (1977). *Proc. 5th International Conference on High-Voltage Electron Microscopy, Kyoto*, pp. 321–324. Tokyo: Japanese Society of Electron Microscopy.
MATSUI, Y., HORIUCHI, S. & OHTA, T. (1980). *J. Solid State Chem.* **32**, 181–184.
PAULING, L. (1960). *The Nature of the Chemical Bond*, 3rd ed., pp. 505–562. Ithaca: Cornell Univ. Press.
SATO, H. & HIROTSU, Y. (1976). *Mater. Res. Bull.* **11**, 1307–1317.
SCHERZER, O. (1949). *J. Appl. Phys.* **20**, 20–29.
WEBER, N. & VENERO, A. F. (1970). Paper 1-JV-70, 72nd Annual Meeting of Am. Ceram. Soc., Philadelphia.
YAMAGUCHI, G. & SUZUKI, K. (1968). *Bull. Chem. Soc. Jpn*, **41**, 93–99.

Acta Cryst. (1981). A**37**, 61–65

Stacking Variants for Doubly-Connected Systems Arranged According to the Percentages of Hexagonal Stacking

BY K. KLEPP AND E. PARTHÉ

Laboratoire de Cristallographie aux Rayons X, Université de Genève, Quai Ernest Ansermet 24, *CH*-1211 *Genève* 4, *Switzerland*

(*Received* 21 *May* 1980; *accepted* 1 *July* 1980)

Abstract

As an extension of Table 7.1.5*B* of *International Tables for X-ray Crystallography* [(1967), Vol. II. Birmingham: Kynoch Press], the possible stacking variants up to ten layers are arranged according to the percentage of hexagonal stacking. A method is given which allows one to calculate the number of possible stacking variants for any number of layers.

Introduction

Over the last few years several relations have been found between certain physical or structural properties and the percentage of hexagonal stacking of the layers or sheets for compounds which have close-packed or derivative structures.

The following examples can be mentioned:

(*a*) The change in the percentage of hexagonal stacking of close-packed rare-earth metals, R, or of rare-earth–aluminium alloys, RAl_3, with increasing pressure (Gschneidner & Pearson, 1968).

(*b*) The change of the birefringence of ZnS variants with a change of the percentage of hexagonal stacking (Brafman & Steinberger, 1966; Parthé, 1972).

(*c*) The change of the percentage of hexagonal stacking of ternary Laves phases with valence electron concentration (Parthé, 1974; Komura & Kitano, 1977).

0567-7394/81/010061-05$01.00